Published in final edited form as:
J Magn Reson Imaging. 2014 May ; 39(5): 1161–1170. doi:10.1002/jmri.24266.

Vascular Masking for Improved Unfolding in 2D SENSE-Accelerated 3D Contrast-Enhanced MR Angiography

Eric G. Stinson, MS[1], **Eric A. Borisch, MS**[1], **Casey P. Johnson, PhD**[2], **Joshua D. Trzasko, PhD**[1], **Phillip M. Young, MD**[3], and **Stephen J. Riederer, PhD**[1]

[1]Mayo Clinic, MR Laboratory. Rochester, Minnesota, United States

[2]University of Iowa, Radiology. Iowa City, Iowa, United States

[3]Mayo Clinic, Radiology. Rochester, Minnesota, United States

Abstract

Purpose—To describe and evaluate the method we refer to as “vascular masking” for improving signal-to-noise ratio (SNR) retention in SENSE-accelerated contrast-enhanced MR angiography (CE-MRA).

Materials and Methods—Vascular masking is a technique which restricts the SENSE unfolding of an accelerated subtraction angiogram to the voxels within the field of view known to have enhancing signal. This is a more restricted voxel set than that identified with conventional masking which excludes only voxels in the air around the object. Thus, improved retention of SNR is expected. Evaluation was done in phantom and in vivo studies by comparing SNR and the g-factor in results reconstructed using vascular vs. conventional masking. A radiological evaluation was also performed comparing conventional and vascular masking in R = 8 accelerated CE-MRA studies of the thighs (n=21) and calves (n=13).

Results—Images reconstructed with vascular masking showed significant reduction in g-factor and improved retention of SNR vs. those reconstructed with conventional masking. In the radiological evaluation vascular masking consistently provided reduced background noise, improved luminal signal smoothness, and better small vessel conspicuity.

Conclusion—Vascular masking provides improved SNR retention and improved depiction of the vasculature in accelerated, subtraction 3D CE-MRA of the thighs and calves.

Keywords

Contrast-enhanced MR angiography (CE-MRA); SENSE; masking

INTRODUCTION

Parallel imaging methods such as sensitivity encoding (SENSE) (1) and GeneRalized Autocalibrating Partially Parallel Acquisitions (GRAPPA) (2) have provided gains in imaging speed since their introduction over a decade ago. A major application of parallel imaging has been in contrast-enhanced MR angiography (CE-MRA) (3–15). Using 2D SENSE acceleration (16) with complex subtraction, recent work has demonstrated acceleration factors of R = 8 or higher (17, 18). Such high acceleration factors in CE-MRA are critical when performing studies where high spatial resolution and temporal information

Corresponding Author and Reprint Info: S.J.R., 200 First Street SW, Rochester, MN 55905. Telephone / Fax: (507) 284 6209 / (507) 284 9778, Riederer@mayo.edu.

is desired, such as fluoroscopic tracking (19), multi-station studies, or imaging fast filling structures such as arteriovenous malformations(20). Reductions in scan time, however, come at the expense of reduced signal-to-noise ratio (SNR) from the reduction in the number of acquired k-space samples and noise amplification indicated by g-factor (1). In the original descriptions of SENSE (1, 16), the exclusion of non-signal-producing voxels in air was shown to reduce g-factor and improve local SNR. Specifically, signal producing voxels (tissue) are included in the SENSE unfolding process, and voxels that are known to have zero signal (air) are excluded. In this work, this masking method is referred to as "conventional masking."

CE-MRA, whether accelerated or not, often emphasizes enhanced voxels by subtracting a static tissue reference image from the subsequent contrast-enhanced time frames (21–24). With an ideal subtraction, the resulting difference image contains true non-zero signal only within the contrast-enhanced vasculature, and no true signal in the remaining, non-perfusing static tissue voxels. Thus, subtracted CE-MRA presents the opportunity to further reduce the degree of aliasing and hence g-factor-related SNR loss by masking out static tissue voxels before the SENSE unfolding of the subtracted, aliased contrast-enhanced image.

The purpose of this work is to describe the method we refer to as "vascular masking" for providing improvement of SNR in accelerated CE-MRA. This is achieved by excluding non-enhancing tissue voxels from the SENSE unfolding process. The methodology and experimental results are presented for phantom and in vivo CE-MRA studies.

MATERIALS AND METHODS

Motivation

Consider in Figure 1 the hypothetical example of $R = R_Y \times R_Z = 4 \times 2$ 2D SENSE acceleration for 3D CE-MRA of the abdomen as used in reference (25). R_Y and R_Z are defined as the acceleration factors along the Y and Z directions, respectively. Assume the number of coil elements is $N_C = 8$, and the potential number of aliased voxels is $N_A = 8$. The sensitivity matrix has size $N_C \times N_A$, and without masking has size 8×8. SENSE unfolding then comprises solving eight equations for eight unknowns. With conventional masking (a), three voxels are excluded as air, and because these zero values are not aliased onto other points, the coil sensitivity matrix size is reduced to 8×5 – eight equations and five unknowns. In the proposed vascular masking case (b), four voxels are additionally excluded as non-enhancing static tissue, and only one voxel remains as vascular signal. With eight equations and one unknown, the system of equations is maximally overdetermined, and the linear least squares solution has maximal degrees of freedom for SNR optimization. In this example only one voxel contained vascular signal, but in general there may be more vascular voxels per aliasing group. The goal is to maximize the degrees of freedom of the solution by removing all non-vascular voxels from the system of equations.

The concepts above can be expressed mathematically. Local SNR of an accelerated acquisition, SNR_{accel}, is related to the SNR of a fully sampled acquisition, SNR_{full}, by Equation 1.

$$SNR_{accel} = \frac{SNR_{full}}{g\sqrt{R}} \quad [1]$$

where R is the reduction in the number of k-space samples, and g is the geometry factor (g-factor), defined as,

$$g_j = \sqrt{[(S^H \psi^{-1} S)^{-1}]_{j,j} [S^H \psi^{-1} S]_{j,j}} \quad [2]$$

where S is the coil sensitivity encoding matrix, S^H is its conjugate transpose, and ψ is the noise covariance matrix. As stated previously, masking allows removal of columns of S, yielding a submatrix of $S^{H\psi^{-1}}S$ with reduced order.

That masking improves the mean square error (MSE) of SENSE reconstruction can be readily proven using standard linear algebraic tools. For brevity, this proof is not included. However, unlike SNR, MSE only assesses global reconstruction performance. Pruessmann et al. (1) conjectured that the exclusion of non-signal-producing voxels from the SENSE unfolding process improved local SNR.

Numerical simulations were performed to show that as the sensitivity encoding matrix S is reduced in size, the associated g-factor is not increased. Figure 2 shows the results of creating 2^{13} random 8 × 8 real-valued coil sensitivity matrices and calculating the g-factor (assuming ψ is equal to the identity matrix) for (i) no mask (S has size 8 × 8) (ii) a conventional mask (In this example, S was chosen to have size 8 × 5), and (iii) a vascular mask (Here, S was chosen to have size 8 × 1). The resulting g-factors were then sorted according to those found without a mask and plotted. The g-factors calculated from the reduced sensitivity matrix are never seen to be greater than those of the full sensitivity matrix. Thus, provided masking does not cause inaccuracies of its own, it can reduce the mean square error, g-factor, and improve SNR_{accel} in Equation 1.

Reconstruction Framework

SENSE unfolding with conventional masking typically distinguishes tissue from air by thresholding a sum-of-squares of the fully sampled coil sensitivity images to exclude the voxels within air (1). A flowchart of one possible variation of SENSE-accelerated CE-MRA reconstruction with conventional masking is shown in Figure 3a. The raw coil sensitivity data is Fourier transformed from k-space to image space to obtain coil sensitivity images and an anatomical voxel exclusion mask. A complex subtraction is performed (26, 27) to subtract the accelerated static tissue raw data from each accelerated CE-MRA time frame data set in k-space and the subtracted data is then transformed to image space to obtain each aliased, subtracted image. The subtraction step can occur at any stage during the reconstruction, whether in k-space, image space, or after the SENSE unfolding. Finally, each of these images, along with the coil sensitivity images and the voxel exclusion mask are used in the SENSE unfolding process to obtain the unfolded, subtracted angiogram.

Reconstruction with a vascular mask is performed by applying two additional steps, shown in Figure 3b, to the conventional SENSE unfolding just described. First, a vascular mask is generated from the subtracted, unfolded image reconstructed using conventional masking. Second, using the same raw k-space data and coil sensitivities as for conventional SENSE unfolding, the SENSE unfolding is repeated using the more restrictive vascular mask.

Vascular Mask Selection Algorithm

In contrast with vascular tree segmentation where a skeleton structure is of interest, the goal of the vascular mask algorithm is to remove subtracted static tissue voxels from the SENSE unfolding while avoiding the exclusion of true vessels. Any vessels that are incorrectly removed (i) will not be present in the final angiogram, and (ii) may falsely deposit their signal to an unmasked voxel within the same aliased voxel group. To this effect, two preventive methods were used in this work:

1. When possible, the next-future time frame (n + 1) from a time-resolved study was used for masking frame n. The future time frame was generally further enhanced, and thus included more vessels than were present in the time frame to be reconstructed. Additionally, the enhanced vessels were usually more intense in the next-future time frame, simplifying vessel masking.
2. The mask was dilated after creation. This step had the dual effect of connecting any disjoint vessels and widening and extending existing vessels – both important to avoid excluding any enhanced voxels. In this work, the structuring element was a cube measuring five pixels per side. It should be noted that this step does not dilate the vessels themselves, but simply allows more voxels to be included in the SENSE unfolding.

Vessel segmentation in SENSE-reconstructed angiograms is challenging due to the non-uniform distribution of noise in the image. Typically, expectation maximization (28), region growing (29), or level set (30–32) algorithms are used to separate vessels from the background. In this work the following semi-automatic technique was used because it showed robust performance in the presence of non-uniform noise. First, an appropriate starting axial partition was manually chosen in which the strongly-enhanced vascular signal could be easily differentiated from background signal. In the thighs, for example, this axial slice was at the superior aspect of the external iliac arteries. Second, the selected axial slice was manually thresholded to segment the arteries. Third, the segmentation was extended to the full volume one axial slice at a time based on three criteria:

1. Absolute proximity to previously segmented voxels
2. Normalized intensity within the slice
3. Ratio of normalized proximity to mean intensity within the slice

When the proximity of a voxel was found to be within a user-defined radius, the normalized intensity was greater than a user-defined limit, and the ratio of normalized proximity to mean intensity was less than a user-defined limit, that voxel was classified as a vascular voxel. The user-defined limits were chosen individually for each study. Criteria 1 and 2 were chosen under the assumptions that voxels that are close to known vessels and comparatively intense within the slice are likely to be vascular voxels. Criterion 3 was included to account for signal falloff in superior and inferior slices at the edges of the longitudinal field of view (FOV), where low signal and amplified noise confounded Criteria 1 and 2.

The vascular-masked image eliminates considerable background material, and so to provide an anatomical reference for radiological evaluation, a composite image was formed by combining the static tissue signal from the conventionally masked reconstruction with the vascular signal from the angiogram reconstructed with the vascular mask. This is achieved by creating a difference mask between the conventional and vascular masks, multiplying the conventionally reconstructed volume by this difference mask, and adding that result to the angiogram reconstructed with the vascular mask. This step has the additional benefit of replacing any vessels that may have been inadvertently excluded by vascular masking, although in their conventionally masked reconstruction form.

Phantom Experiments

A bovine gelatin phantom designed to simulate a longitudinal vessel within static background tissue was used to study the effect of vascular masking under controlled conditions. The phantom had left/right (L/R) and anterior/posterior (A/P) dimensions of 19 × 19 cm^2 and was 10 cm long in the superior/inferior (S/I) direction. Within it, the phantom

had a 1.9 cm diameter cylindrical void along the S/I direction into which a 1.7 cm diameter vial of plain gelatin or Gadolinium-doped gelatin was inserted to simulate a vessel in its unenhanced or enhanced state, respectively. Fully sampled and SENSE-accelerated 3D T1-weighted images were acquired in the coronal format with phase and slice encoding in the axial plane. The FOV and resolution, shown in Table 1, were chosen to mimic the typical filling of the FOV by an abdomen (25). Two acquisitions were performed to simulate the unenhanced and contrast-enhanced frames – one with the unenhanced vial present and one with the Gadolinium-doped vial present. Seven sets of acceleration factors were used for each data set: $R_Y \times R_Z = 1 \times 1, 2 \times 1, 3 \times 1, 4 \times 1, 2 \times 2, 3 \times 2, 4 \times 2$. Image reconstructions were performed at each acceleration with: (i) no mask, (ii) conventional anatomical mask, (iii) newly-proposed vascular mask. The vascular mask was chosen to loosely fit the simulated vessel such that a region of interest (ROI) large enough to measure background noise could be drawn outside of the enhanced vial but still within the unmasked background. Signal, noise, and g-factor were measured in ROIs in a single central axial slice of the phantom. The signal and noise ROIs encompassed 144 and 4683 pixels, respectively. The g-factor maps were calculated from the coil sensitivity images using each type of masking, and mean values were measured as an average over both the signal and noise ROIs. The SNR was measured in the fully sampled, unaccelerated volume and then adjusted according to Equation 1 using the known *R* and measured mean g-factor values to estimate the reduced SNR of each accelerated scan.

In Vivo Experiments

To test the effect of vascular masking in vivo, 21 thigh studies and 13 calf studies, all acquired using R = 8 2D SENSE-accelerated CE-MRA with the CAPR method (17, 19, 33), were retrospectively reconstructed with the proposed method. All studies were IRB approved. These particular studies were chosen such that, by casual visual inspection the full-FOV maximum intensity projections (MIPs) from a conventional mask reconstruction showed few artifacts from misregistration between the pre-contrast reference image and the contrast-enhanced image and thus were near-ideal subtractions, fitting a key assumption of the vascular masking technique. Typical scan parameters and demographic data for each anatomic region are shown in Table 1. Additionally, 2D homodyne undersampling was used in these studies, giving an additional scan time reduction by the homodyne factors shown in Table 1. Each study was reconstructed with both the conventional and vascular masking techniques. This type of retrospective study was possible because in all studies the original data and coil sensitivity images had been archived.

Empirical SNR and g-factor analyses were performed for each in vivo study by drawing signal and noise ROIs containing ten consecutive 1.0 mm or 1.5 mm thick axial partitions in the femoral artery of the thighs (n = 20 right and n = 1 left) and the anterior tibial artery (n = 8 right and n = 5 left) in the calves. Sections of the arteries were chosen such that there was adequate unmasked background signal around the vessel in the vascular mask for a sizable noise ROI without including branching arteries. Paired Student's t-tests (34) were used to determine the significance of any empirical SNR improvement for vascular vs. conventional masking, where the percent change in SNR between masking techniques was calculated for each study individually.

To further aid our understanding of the vascular masking technique, the percent of FOV filling and number of aliases were evaluated with both conventional and the new vascular masking. For each slice, the alias count for each voxel was determined, where the alias count is defined as the number of voxels from throughout the full-FOV superimposed onto a voxel in the aliased image. An alias count of zero for a voxel means that the voxel has been masked out. An alias count of one means that a voxel has not been masked out and has no

other voxels aliased onto it. The number of voxels with alias counts greater than zero gives the number of unmasked voxels in a slice.

Radiologic Evaluation

Image results from the in vivo studies were used to test the hypothesis that reconstruction with a vascular mask provides improved image quality compared to reconstruction with a conventional mask. Images reconstructed with each of the masks were evaluated with respect to the categories specified in Table 2 by the collaborating radiologist (P.M.Y.). Specifically, the conventionally masked images were compared to the composite of the vascularly masked reconstruction and conventionally masked background as described above. Due to the obvious differences in the images produced by the different reconstructions, no attempt was made to make the study blind. The radiologist was provided with the original coronal partitions for all studies and had the ability to reformat and create MIPs as needed for evaluation.

The “no improvement” state was chosen as the null hypothesis for each evaluation category. That is, in Category I, the null hypothesis encompasses scores of −2 , −1, and 0, and the alternate hypothesis encompasses 1 and 2. In Category II, the null hypothesis is a score of 1, and the alternate is a score of 0. And in Category III, the null hypothesis is a score of −1 or 0, and the alternate is a score of 1. Therefore, a one-sided Wilcoxon signed rank test (35) was used to test for significance in Categories I and III, and a two-sided Wilcoxon signed rank test was used for Category II. Significance was taken as $P < 0.05$.

RESULTS

Phase-encode plane partitions of reconstruction masks, image slices, and g-factor maps for an R = 4 × 2 accelerated scan of the bovine gelatin phantom are shown in Figure 4. Using more restrictive masks, the same raw data is reconstructed into images with reduced noise. The reduced noise amplification is also apparent in the g-factor maps which show greatly reduced g-factors when more restrictive masks are used. Note that the vascular mask in the phantom experiment is larger than was used in vivo to allow for noise analysis.

Figure 5 shows mean g-factor measurements and estimated SNR of the phantom images for the range of investigated accelerations for each of the reconstructions with no mask, the conventional mask, and the vascular mask. The SNR of the images reconstructed with the vascular mask improved at all accelerations compared to those reconstructed without masking or with the conventional mask. When using the vascular mask, for all but the highest R_Y, the measured g-factor approaches unity, and the estimated SNR approaches the theoretical SNR predicted from Equation 1 with a g-factor of unity.

Histograms of the scores given to the in vivo images during radiological review are shown in Figure 6. For Categories I (major vessel depiction) and III (overall assessment) vascular masking provided statistically significant improvement over conventional masking, and there was no significant loss of small vessels due to masking (Category II).

Full-FOV and targeted MIPs of representative thigh and calf studies are shown in Figure 7 and Figure 8. Note the overall reduction of noise amplification and the resultant improvements in luminal signal smoothness (arrowheads) and small vessel conspicuity (arrows). Figure 7 also shows representative axial slices showing the reduction of unmasked voxels used in the SENSE reconstruction (c, f).

Paired plots of SNR and g-factor measurements for the in vivo thigh and calf studies are shown in Figure 9. Compared to conventional masking, the SNR for 21 thigh studies and 13

calf studies reconstructed using the vascular mask significantly increased by 35±6% ($P < 0.001$) and 25±11% ($P < 0.05$), respectively. The measured g-factors in the region of interest were also significantly reduced by using the vascular mask. Over all of the studies, g-factor was reduced by an average of 47±4% (from 2.30 to 1.11, $P < 0.001$) in thighs and 25±6% (from 1.52 to 1.03, $P < 0.01$) in the calves.

The plots of Figure 10 compare the alias counts per axial slice using conventional (a) and vascular (b) masking for the thigh study of Figure 7. Note that the largest number of aliases with the vascular masking technique is only 6, compared to 8 with the conventional mask. Additionally, the number of highly aliased pixels (alias count ≥ 5) has been greatly reduced. Figures 10c–d show similar results for a calf study.

DISCUSSION

This work demonstrates a reconstruction scheme to improve SNR in SENSE-accelerated subtracted CE-MRA. Specifically, the vascular masking technique described here reduces g-factor and improves local SNR by removing subtracted static tissue voxels from the SENSE-unfolding process in addition to the non-signal-producing voxels in air removed with conventional masking. As seen in the phantom studies, reduction in the number of aliased points improved the g-factor and increased local SNR. In the radiological evaluation of 34 CE-MRA studies of the thighs and calves, the improvement was manifest as reduced background noise, improved luminal signal smoothness, and better small vessel conspicuity.

The phantom studies show that vascular masking improves SNR and drives g-factor towards unity. At lower R_Y accelerations the g-factor approaches and achieves unity; however, at high R_Y accelerations ($R_Y > 4$) the g-factor is reduced, but not to g = 1. This is due to an alias count greater than 1 in the highly accelerated case – even when using the vascular mask. While the g-factors at high R_Y acceleration factors do not reach unity, they do improve with any amount of masking. For example, in the case of 4 × 1 SENSE acceleration the mean g-factor improves from 3.86 for reconstruction with no mask to 3.68 for conventional masking and 1.39 for the vascular mask.

Vascular masking was shown to provide significant radiological improvement in both thigh and calf studies, although the improvement was more apparent in the thighs. Conventional masking already accounts for the relatively limited filling of the FOV typical in calf CE-MRA, and any further reduction from vascular masking is comparatively small. The thighs fill a large fraction of the FOV and contain a greater ratio of static tissue to vascular tissue, even with conventional masking; it is therefore more beneficial to further mask subtracted static tissue within the thighs. This can be seen in Figure 10a vs. 10c, in which the alias count of the calf study (Figure 10c) is already limited by using conventional masking compared to the thigh study (Figure 10a).

Vascular masking was implemented for 3DFT/SENSE reconstruction, but similar motivations have driven previous work in backprojection and compressed sensing-based reconstructions (36–38). The method may potentially be adopted to highly accelerated CE-MRA with GRAPPA (27). HighlY constrained back PRojection with Local Reconstruction (HYPR LR) reconstructs each frame of a time series of contrast-enhanced angiograms using a masked backprojection procedure (36), only in a local area of interest (37). k-t Iterative Support Detection (k-t ISD) aims to improve a compressed sensing reconstruction by detecting the locations of nonzero signal (in *x-f* space) during the reconstruction (38). Reference (39) employs a vessel adapted regularization term to improve a compressed-sensing reconstruction. Like vascular masking, each of these methods uses prior or online-learned knowledge of the location of nonzero signal to improve upon a reconstruction

scheme. Like k-t ISD, vascular masking also lends itself to iteration, and can be repeated until appropriate stopping criteria are met. In practice, however, reconstruction performance improves significantly even if only one iteration is executed, and only this base case was considered in this work.

Contrast-enhanced angiograms of the thighs and calves were targeted in this study because they often provide near-ideal subtractions, with few artifacts from motion between the reference and contrast-enhanced scans. Appropriate studies are easily identified by the absence of large regions of bright signal in non-vascular regions of the difference images. This assumption is required for any technique involving masking for improved SENSE unfolding. If the assumption of a near-ideal subtraction (near zero movement) is broken and the poor subtraction regions are erroneously excluded in the mask, the unfolding process could cause an artifact by incorrectly depositing the energy from the excluded voxel to another voxel. Therefore, the effectiveness of vascular masking in its current form is limited in regions such as the thorax and abdomen, where motion is likely. In the abdomen specifically, poor breath holds and bowel motion preclude the use of this technique. Solutions to allow application to these more difficult anatomies could accommodate motion artifacts in the reduced mask, and partially benefit from the vascular masking technique without the risk of introducing unfolding artifacts.

The current masking algorithm may incorrectly exclude truly enhancing, perfusing tissue if used during later time frames of a contrast-enhanced study. Reconstruction in such a situation would have the dual deleterious effect of excluding perfusing tissue that is actually enhancing and introducing artifacts elsewhere in the image. Therefore, in its current form the vascular masking method is most appropriate for first-pass arterial imaging. By somehow modifying the masking technique to include perfusing tissue as well as vascular anatomy, these limitations might possibly be avoided, although the efficacy of the vascular masking reconstruction would likely be reduced.

In its current form, the vascular masking algorithm is semi-automatic and requires some user intervention. To gain clinical acceptance, the masking will likely need to be automated. This is the subject of future research.

In conclusion, improved SENSE unfolding has been demonstrated in accelerated subtraction 3D CE-MRA in the thighs and the calves using the technique of vascular masking. Images reconstructed with this technique show reduced noise amplification, improved luminal signal smoothness, and better small vessel conspicuity.

Supplementary Material

Refer to Web version on PubMed Central for supplementary material.

Acknowledgments

Grant Support:

Contract grant sponsor: NIH; Contract grant numbers: EB000212, HL070620, RR018898.

REFERENCES

1. Pruessmann KP, Weiger M, Scheidegger MB, Boesiger P. SENSE: sensitivity encoding for fast MRI. Magn Reson Med. 1999; 42:952–962. [PubMed: 10542355]
2. Griswold MA, Jakob PM, Heidemann RM, et al. Generalized autocalibrating partially parallel acquisitions (GRAPPA). Magn Reson Med. 2002; 47:1202–1210. [PubMed: 12111967]

3. Sodickson DK, McKenzie CA, Li W, Wolff S, Manning WJ, Edelman RR. Contrast-enhanced 3D MR angiography with simultaneous acquisition of spatial harmonics: A pilot study. Radiology. 2000; 217:284–289. [PubMed: 11012458]
4. Weiger M, Pruessmann KP, Kassner A, et al. Contrast-enhanced 3D MRA using SENSE. J Magn Reson Imaging. 2000; 12:671–677. [PubMed: 11050636]
5. Quick HH, Vogt FM, Maderwald S, et al. High spatial resolution whole-body MR angiography featuring parallel imaging: initial experience. Rofo. 2004; 176:163–169. [PubMed: 14872368]
6. Hu HH, Madhuranthakam AJ, Kruger DG, Huston J 3rd, Riederer SJ. Improved venous suppression and spatial resolution with SENSE in elliptical centric 3D contrast-enhanced MR angiography. Magn Reson Med. 2004; 52:761–765. [PubMed: 15389954]
7. Meckel S, Mekle R, Taschner C, et al. Time-resolved 3D contrast-enhanced MRA with GRAPPA on a 1.5-T system for imaging of craniocervical vascular disease: initial experience. Neuroradiology. 2006; 48:291–299. [PubMed: 16532336]
8. Nael K, Saleh R, Lee M, et al. High-spatial-resolution contrast-enhanced MR angiography of abdominal arteries with parallel acquisition at 3.0 T: initial experience in 32 patients. AJR Am J Roentgenol. 2006; 187:W77–W85. [PubMed: 16794143]
9. Wilson GJ, Eubank WB, Vasbinder GB, et al. Utilizing SENSE to reduce scan duration in high-resolution contrast-enhanced renal MR angiography. J Magn Reson Imaging. 2006; 24:873–879. [PubMed: 16941607]
10. Zenge MO, Vogt FM, Brauck K, et al. High-resolution continuously acquired peripheral MR angiography featuring partial parallel imaging GRAPPA. Magn Reson Med. 2006; 56:859–865. [PubMed: 16964615]
11. Brauck K, Maderwald S, Vogt FM, Zenge M, Barkhausen J, Herborn CU. Time-resolved contrast-enhanced magnetic resonance angiography of the hand with parallel imaging and view sharing: initial experience. Eur Radiol. 2007; 17:183–192. [PubMed: 16710664]
12. Nael K, Fenchel M, Krishnam M, Laub G, Finn JP, Ruehm SG. High-spatial-resolution whole-body MR angiography with high-acceleration parallel acquisition and 32-channel 3.0-T unit: initial experience. Radiology. 2007; 242:865–872. [PubMed: 17325071]
13. Xu PJ, Yan FH, Wang JH, Lin J, Fan J. Utilizing generalized autocalibrating partial parallel acquisition (GRAPPA) to achieve high-resolution contrast-enhanced MR angiography of hepatic artery: initial experience in orthotopic liver transplantation candidates. Eur J Radiol. 2007; 61:507–512. [PubMed: 17169520]
14. Nael K, Fenchel M, Krishnam M, Finn JP, Laub G, Ruehm SG. 3.0 Tesla high spatial resolution contrast-enhanced magnetic resonance angiography (CE-MRA) of the pulmonary circulation: initial experience with a 32-channel phased array coil using a high relaxivity contrast agent. Invest Radiol. 2007; 42:392–398. [PubMed: 17507810]
15. Muthupillai R, Douglas E, Huber S, et al. Direct comparison of sensitivity encoding (SENSE) accelerated and conventional 3D contrast enhanced magnetic resonance angiography (CE-MRA) of renal arteries: effect of increasing spatial resolution. J Magn Reson Imaging. 2010; 31:149–159. [PubMed: 20027583]
16. Weiger M, Pruessmann KP, Boesiger P. 2D SENSE for faster 3D MRI. Magma. 2002; 14:10–19. [PubMed: 11796248]
17. Haider CR, Glockner JF, Stanson AW, Riederer SJ. Peripheral vasculature: high-temporal- and high-spatial-resolution three-dimensional contrast-enhanced MR angiography. Radiology. 2009; 253:831–843. [PubMed: 19789238]
18. Haider CR, Riederer SJ, Borisch EA, et al. High temporal and spatial resolution 3D time-resolved contrast-enhanced magnetic resonance angiography of the hands and feet. J Magn Reson Imaging. 2011; 34:2–12. [PubMed: 21698702]
19. Johnson CP, Borisch EA, Glockner JF, Young PM, Riederer SJ. Time-resolved dual-station calf-foot three-dimensional bolus chase MR angiography with fluoroscopic tracking. J Magn Reson Imaging. 2012; 36:1168–1178. [PubMed: 22753021]
20. Mostardi PM, Young PM, McKusick MA, Riederer SJ. High temporal and spatial resolution imaging of peripheral vascular malformations. J Magn Reson Imaging. 2012; 36:933–942. [PubMed: 22674646]

21. Douek PC, Revel D, Chazel S, Falise B, Villard J, Amiel M. Fast MR angiography of the aortoiliac arteries and arteries of the lower extremity: value of bolus-enhanced, whole-volume subtraction technique. Am J Roentgenol. 1995; 165:431–437. [PubMed: 7618572]
22. Adamis MK, Li W, Wielopolski PA, et al. Dynamic contrast-enhanced subtraction MR angiography of the lower extremities: initial evaluation with a multisection two-dimensional time-of-flight sequence. Radiology. 1995; 196:689–695. [PubMed: 7644630]
23. Wang Y, Johnston DL, Breen JF, et al. Dynamic MR digital subtraction angiography using contrast enhancement, fast data acquisition, and complex subtraction. Magn Reson Med. 1996; 36:551–556. [PubMed: 8892206]
24. Leiner T, de Weert TT, Nijenhuis RJ, et al. Need for background suppression in contrast-enhanced peripheral magnetic resonance angiography. J Magn Reson Imaging. 2001; 14:724–733. [PubMed: 11747029]
25. Mostardi PM, Glockner JF, Young PM, Riederer SJ. Contrast-enhanced MR angiography of the abdomen with highly accelerated acquisition techniques. Radiology. 2011; 261:587–597. [PubMed: 21900616]
26. Borisch EA, Haider CR, Grimm RC, Riederer SJ. Subtraction in View-Shared 3D Contrast-Enhanced MRA. In: Proceedings of the 18th Annual Meeting of ISMRM, Stockholm, Sweden. 2010 abstract 2932.
27. Koktzoglou I, Sheehan JJ, Dunkle EE, Breuer FA, Edelman RR. Highly accelerated contrast-enhanced MR angiography: improved reconstruction accuracy and reduced noise amplification with complex subtraction. Magn Reson Med. 2010; 64:1843–1848. [PubMed: 20860003]
28. Wilson DL, Noble JA. An adaptive segmentation algorithm for time-of-flight MRA data. IEEE Trans Med Imaging. 1999; 18:938–945. [PubMed: 10628953]
29. Boskamp T, Rinck D, Link F, Kummerlen B, Stamm G, Mildenberger P. New vessel analysis tool for morphometric quantification and visualization of vessels in CT and MR imaging data sets. Radiographics. 2004; 24:287–297. [PubMed: 14730052]
30. Malladi R, Sethian JA, Vemuri BC. Shape Modeling with Front Propagation - a Level Set Approach. IEEE Trans Pattern Anal Mach Intell. 1995; 17:158–175.
31. Lorigo LM, Faugeras OD, Grimson WE, et al. CURVES: curve evolution for vessel segmentation. Med Image Anal. 2001; 5:195–206. [PubMed: 11524226]
32. Chen J, Amini AA. Quantifying 3-D vascular structures in MRA images using hybrid PDE and geometric deformable models. IEEE Trans Med Imaging. 2004; 23:1251–1262. [PubMed: 15493693]
33. Johnson CP, Haider CR, Borisch EA, Glockner JF, Riederer SJ. Time-resolved bolus-chase MR angiography with real-time triggering of table motion. Magn Reson Med. 2010; 64:629–637. [PubMed: 20597121]
34. Rosner, B. Fundamentals of biostatistics. 5th ed.. Pacific Grove, CA: Duxbury; 2000. p. 275
35. Siegel, S. McGraw-Hill series in psychology. New York: McGraw-Hill; 1956. Nonparametric statistics for the behavioral sciences; p. 75
36. Mistretta CA, Wieben O, Velikina J, et al. Highly constrained backprojection for time-resolved MRI. Magn Reson Med. 2006; 55:30–40. [PubMed: 16342275]
37. Johnson KM, Velikina J, Wu Y, Kecskemeti S, Wieben O, Mistretta CA. Improved waveform fidelity using local HYPR reconstruction (HYPR LR). Magn Reson Med. 2008; 59:456–462. [PubMed: 18306397]
38. Liang D, DiBella EV, Chen RR, Ying L. k-t ISD: Dynamic cardiac MR imaging using compressed sensing with iterative support detection. Magn Reson Med. 2012; 68:41–53. [PubMed: 22113706]
39. Hutter, J.; Grimm, R.; Forman, C.; Hornegger, J.; Schmitt, P. Vessel Adapted Regularization for Iterative Reconstruction in MR Angiography; Melbourne, Australia. Proceedings of the 20th Annual Meeting of ISMRM; 2012. abstract 2541

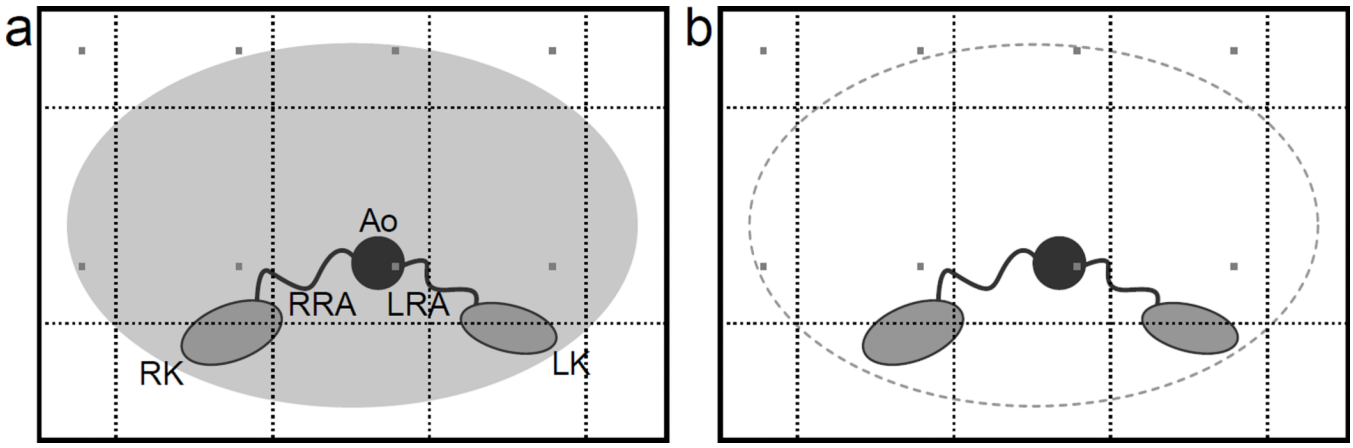

Figure 1.

Diagrams of a conventionally masked (a) and vascular-masked (b) abdomen cross-section with enhanced right and left renal arteries (RRA, LRA), perfused right and left kidneys (RK, LK), and enhanced abdominal aorta (Ao). With 4 × 2 Cartesian SENSE acceleration, a voxel within the aorta is aliased with seven other voxels (gray). Three of the aliased voxels are in air and contain no signal in the unsubtracted case, while in the subtracted case an additional four voxels contain subtracted static tissue. Conventional masking removes the three non-signal-producing aliased voxels in air. In this example, vascular masking removes all seven of the non-signal-producing aliased voxels.

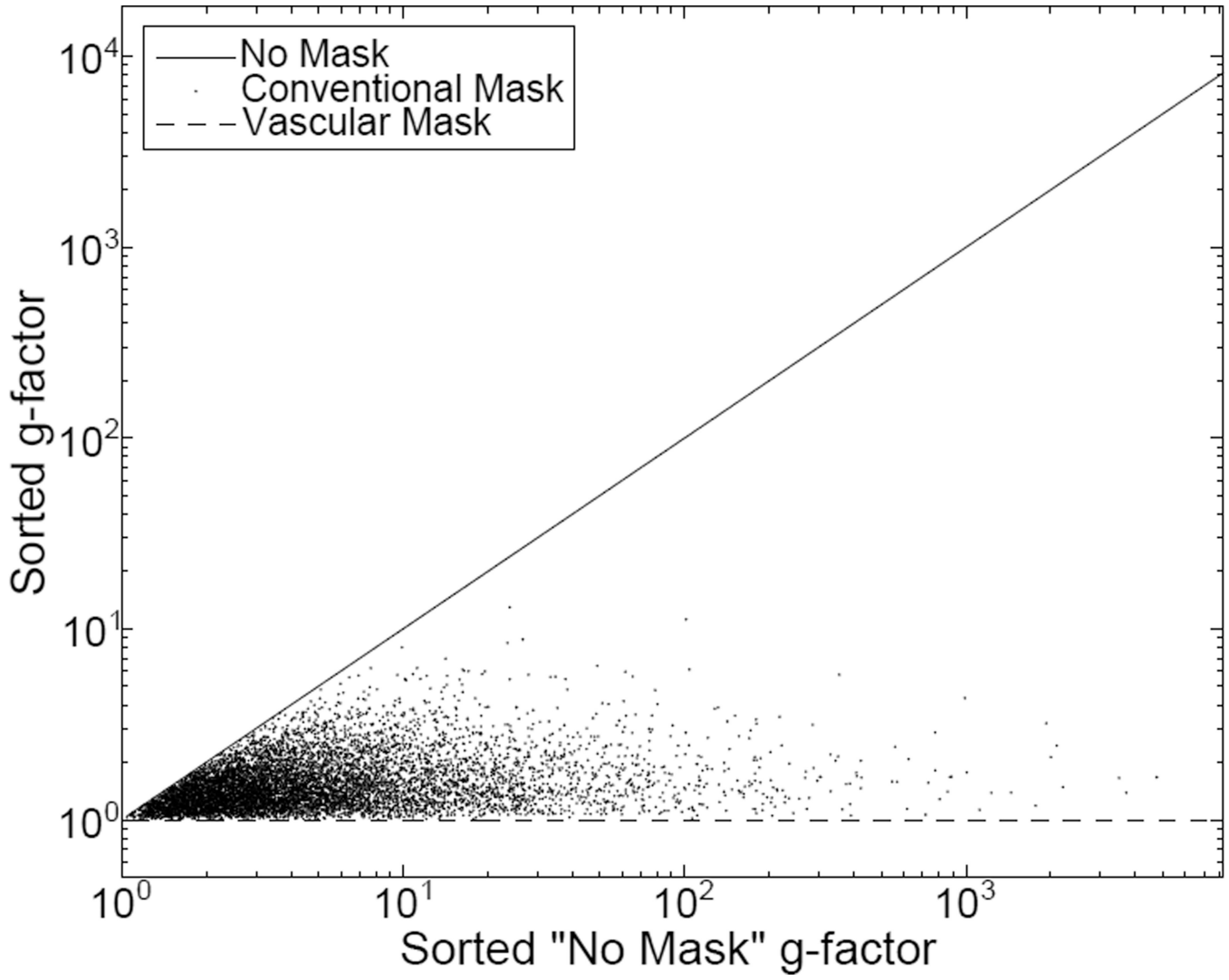

Figure 2.
The g-factors calculated from 2^{13} random sensitivity matrices and sorted according to the g-factor from the reconstruction with no mask. Note that in all cases, reducing the size of the sensitivity matrix by masking reduces the g-factor.

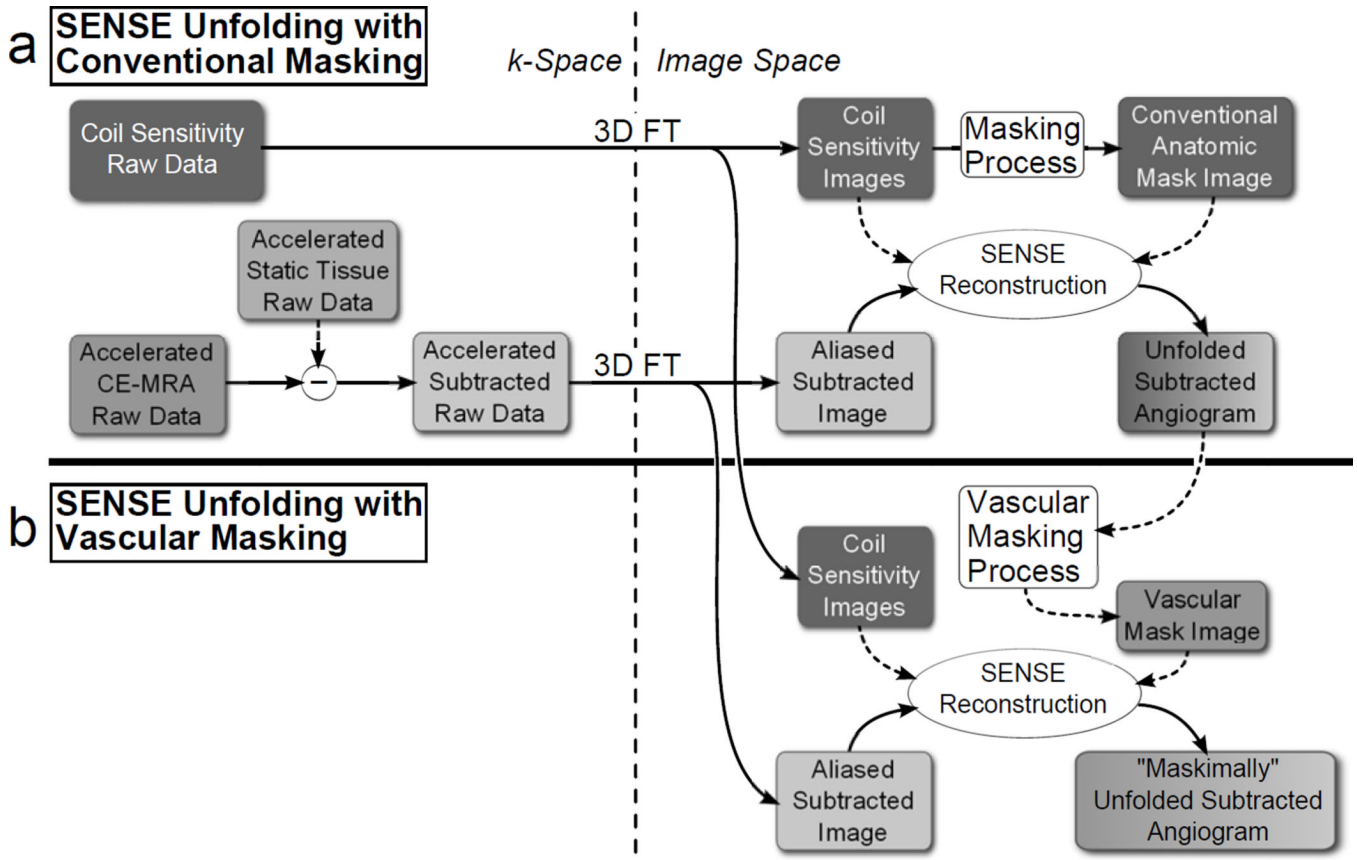

Figure 3.
Flowchart showing the reconstruction process for SENSE unfolding with conventional masking (a) and vascular masking (b). Under the assumption of a near-ideal subtraction, vascular masking uses the result from the conventionally masked reconstruction to create a more restrictive vascular mask to use in the SENSE unfolding.

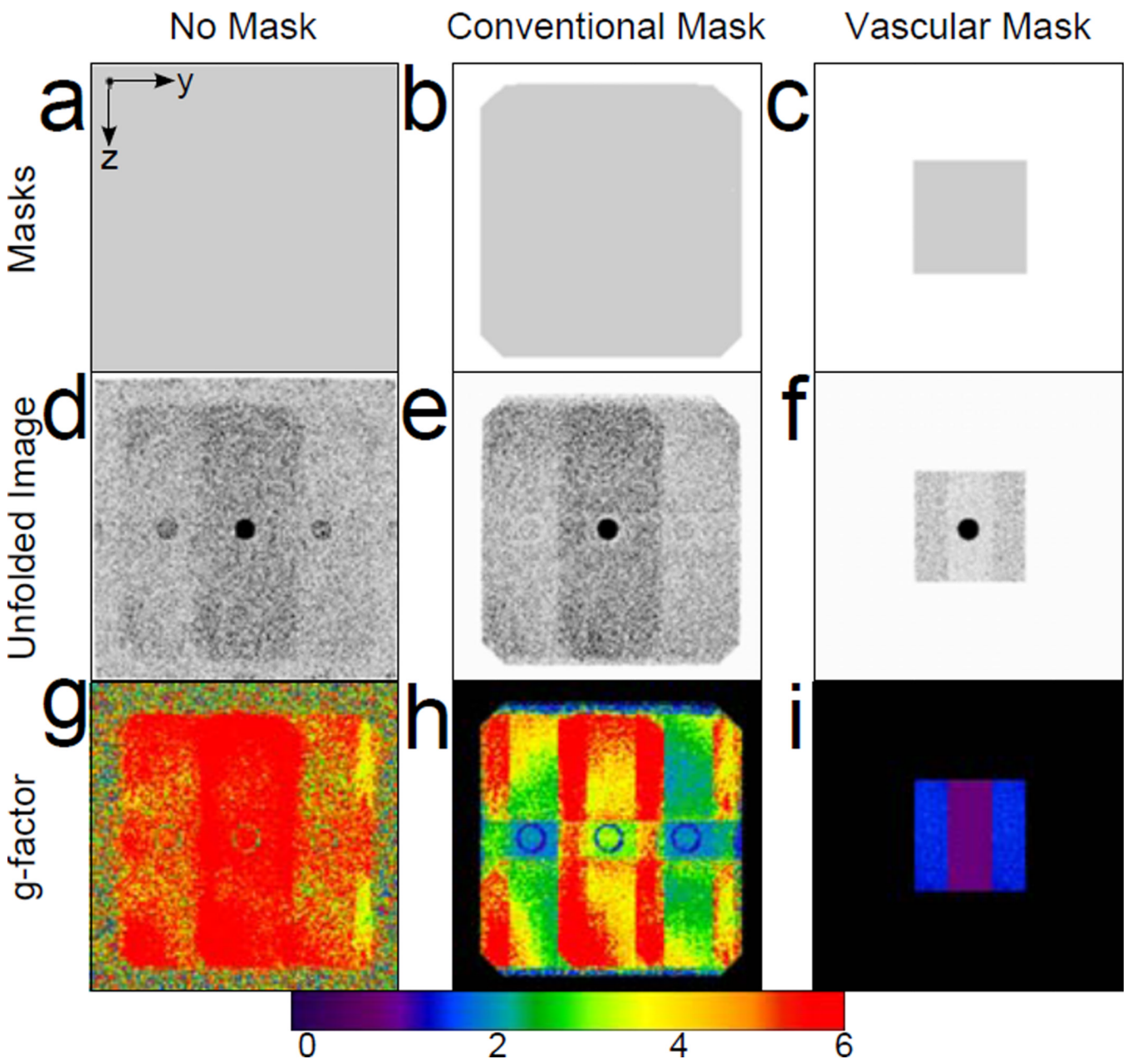

Figure 4.

A phase-encode plane axial partition of an $R_Y \times R_Z = 4 \times 2$ accelerated image of the bovine gelatin phantom shows the difference in masks (a-c), unfolded subtracted images (d-f) and g-factor maps (g-i) for different voxel exclusion masks. Images reconstructed with no mask (a, d, g), the conventional mask (b, e, h), and the vascular mask (c, f, i) are shown.

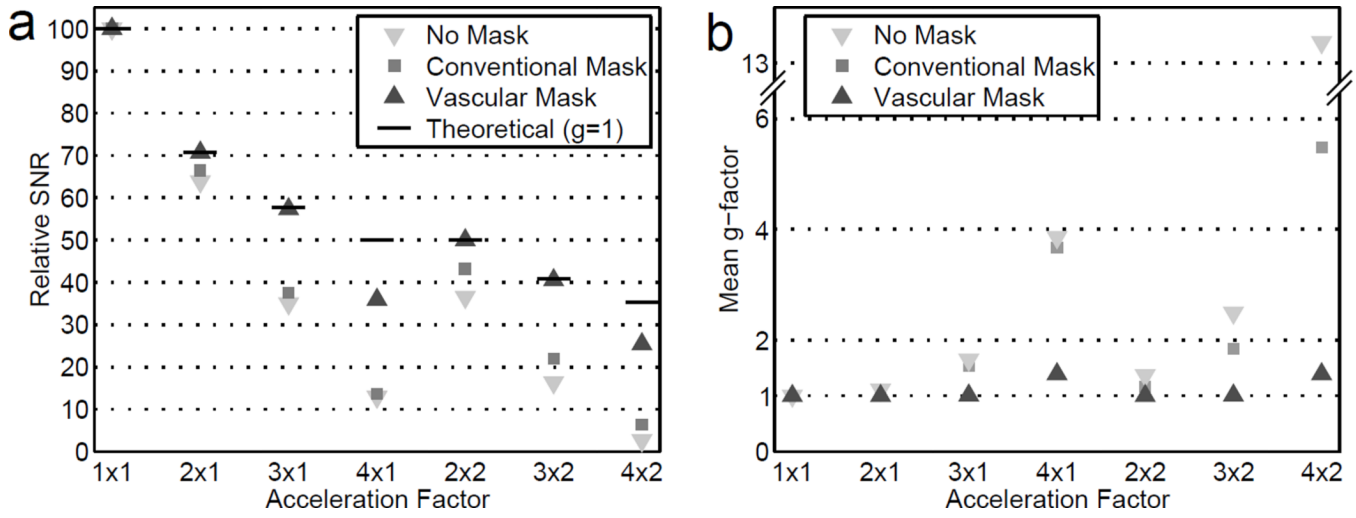

Figure 5.

Relative SNR (a) and mean g-factor (b) in phantom images reconstructed with no mask, the conventional mask, and the vascular mask. The theoretical values in (a) are for g = 1 and $SNR\alpha\frac{1}{\sqrt{R}}$.

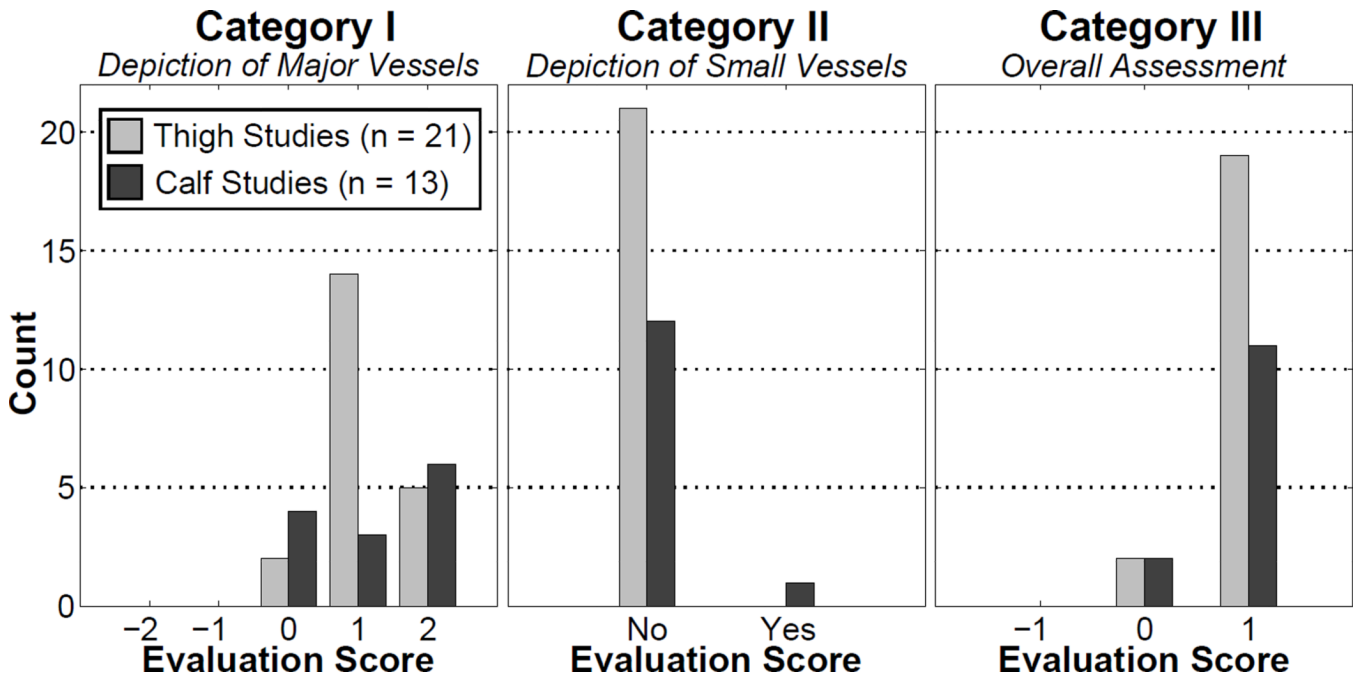

Figure 6.

Histograms of the results of the radiological evaluation for the thigh and calf studies. Categories I – III are defined in Table 2. In Categories I and III, the null hypothesis of "no improvement" was rejected in a statistically significant way, showing that images reconstructed with vascular masking have a radiological improvement compared to images reconstructed with conventional masking. In Category II, there was no significant loss of vessels due to masking.

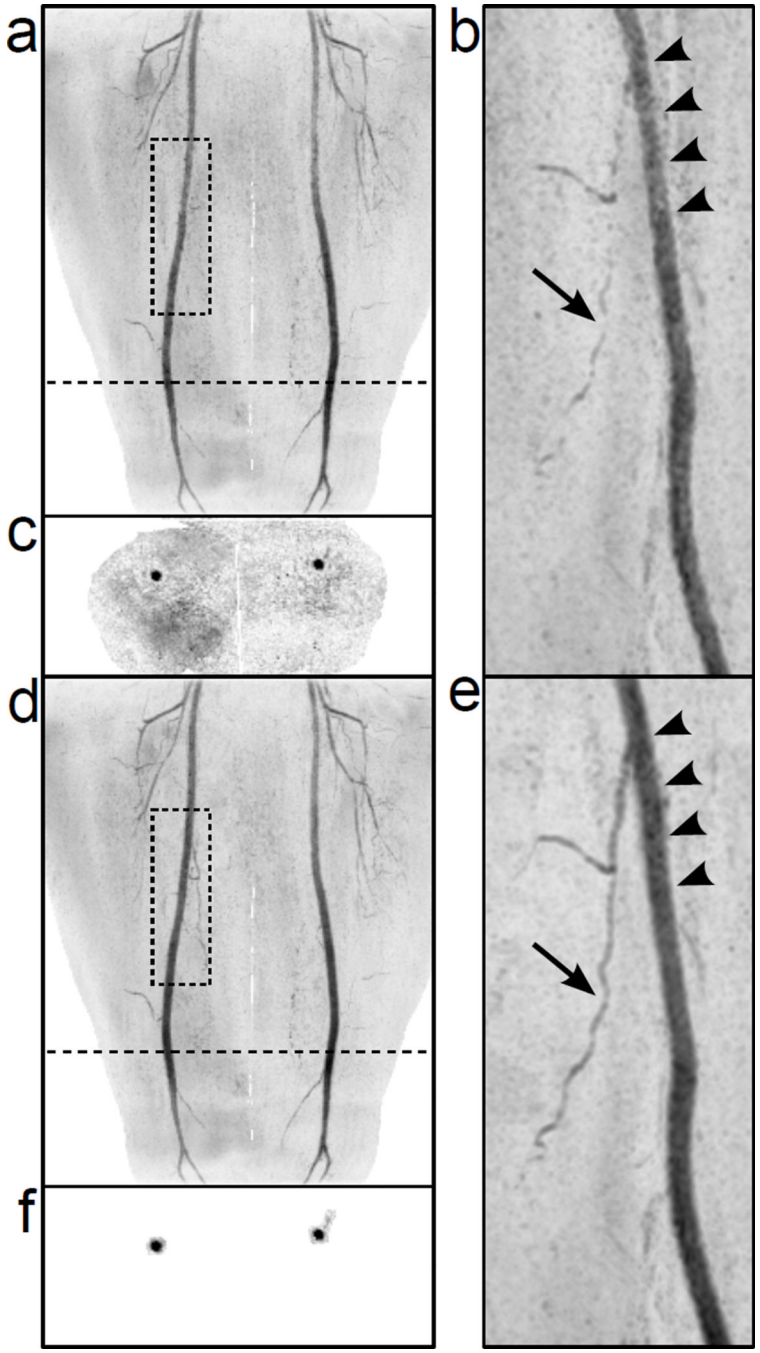

Figure 7.
Full-FOV and rotated targeted MIPs of R = 8 2D SENSE-accelerated 3D CE-MRA thigh angiograms reconstructed with the conventional masking technique (a-b) and the new vascular masking technique (d-e). Representative axial slices of the datasets are shown in (c) and (f). The position of the axial slices is shown by the dotted line on the full-FOV MIPs. The image reconstructed with the vascular mask (e) shows improved luminal signal smoothness (arrow heads) and better small vessel conspicuity (arrow) vs. conventional masking (b).

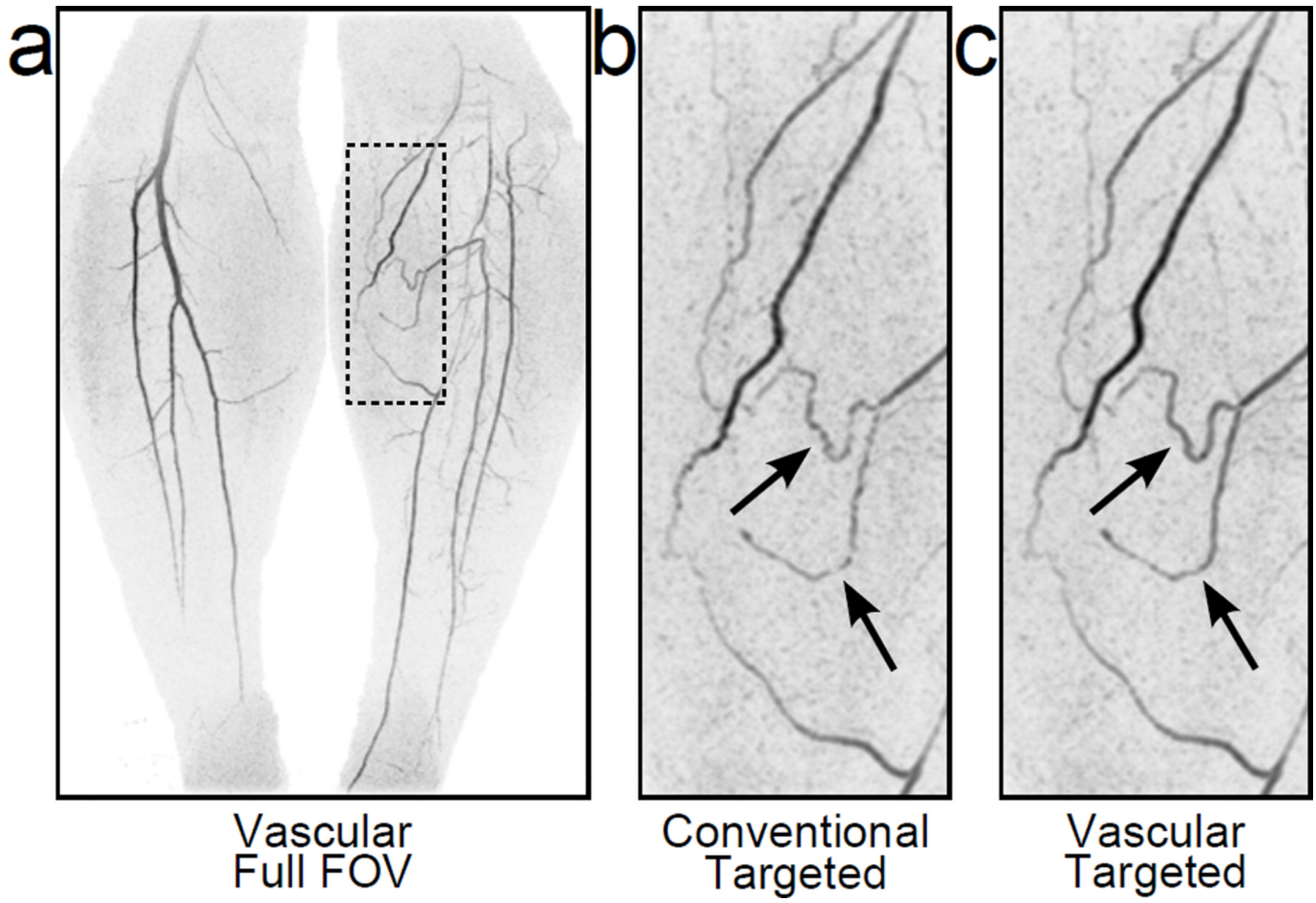

Figure 8.
Full-FOV and targeted MIPs from an R=8 2D SENSE-accelerated 3D CE-MRA calf study reconstructed with the new vascular mask (a, c) and the conventional masking technique (b). Note the improved small vessel conspicuity (arrows) in the image reconstructed using the vascular mask.

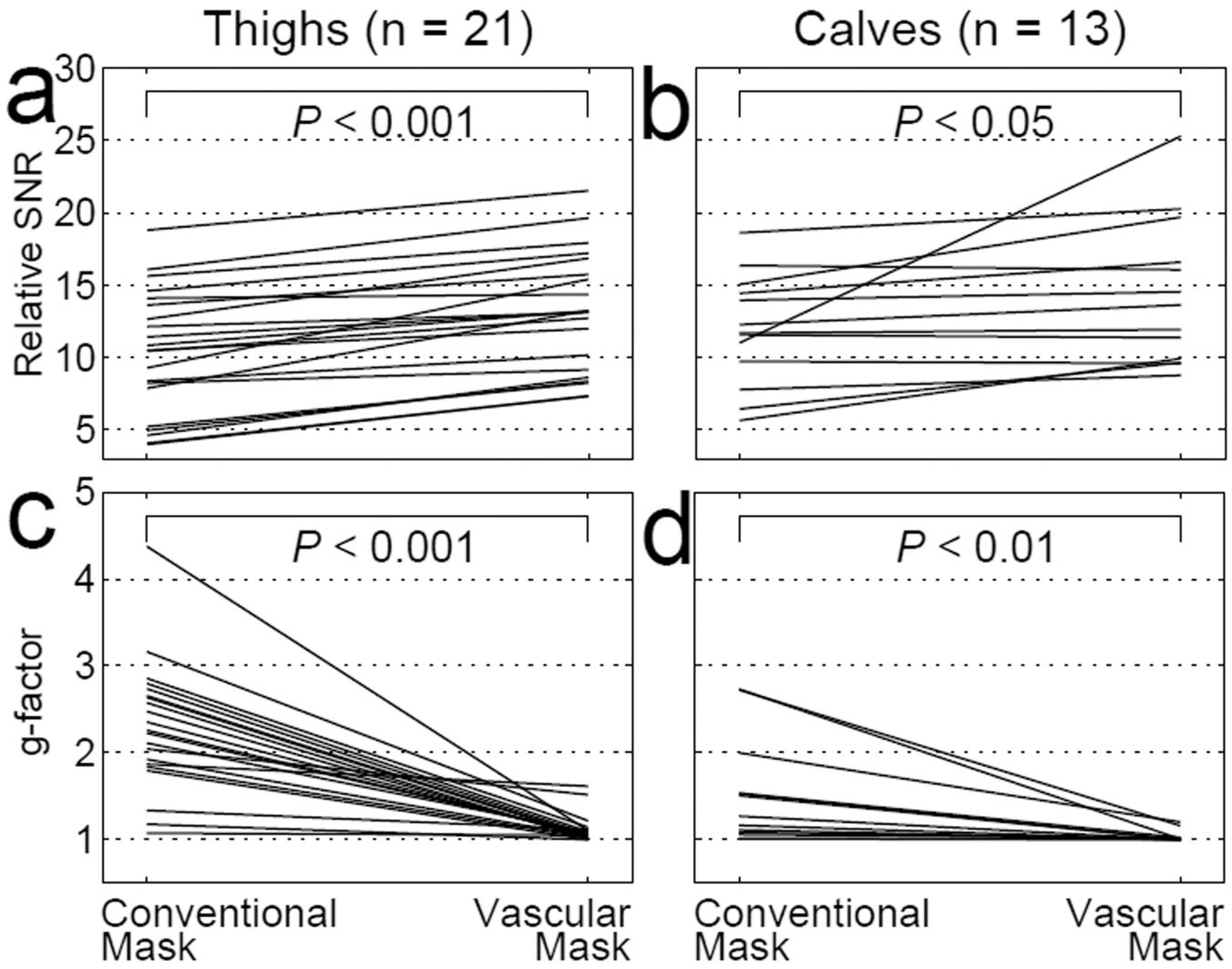

Figure 9.
In vivo relative SNR (a-b) and g-factor (c-d) plots of paired measurements from images reconstructed with the conventional mask and the vascular mask. Thigh results (n = 21) are shown in (a, c), and calf results (n = 13) are shown in (b, d).

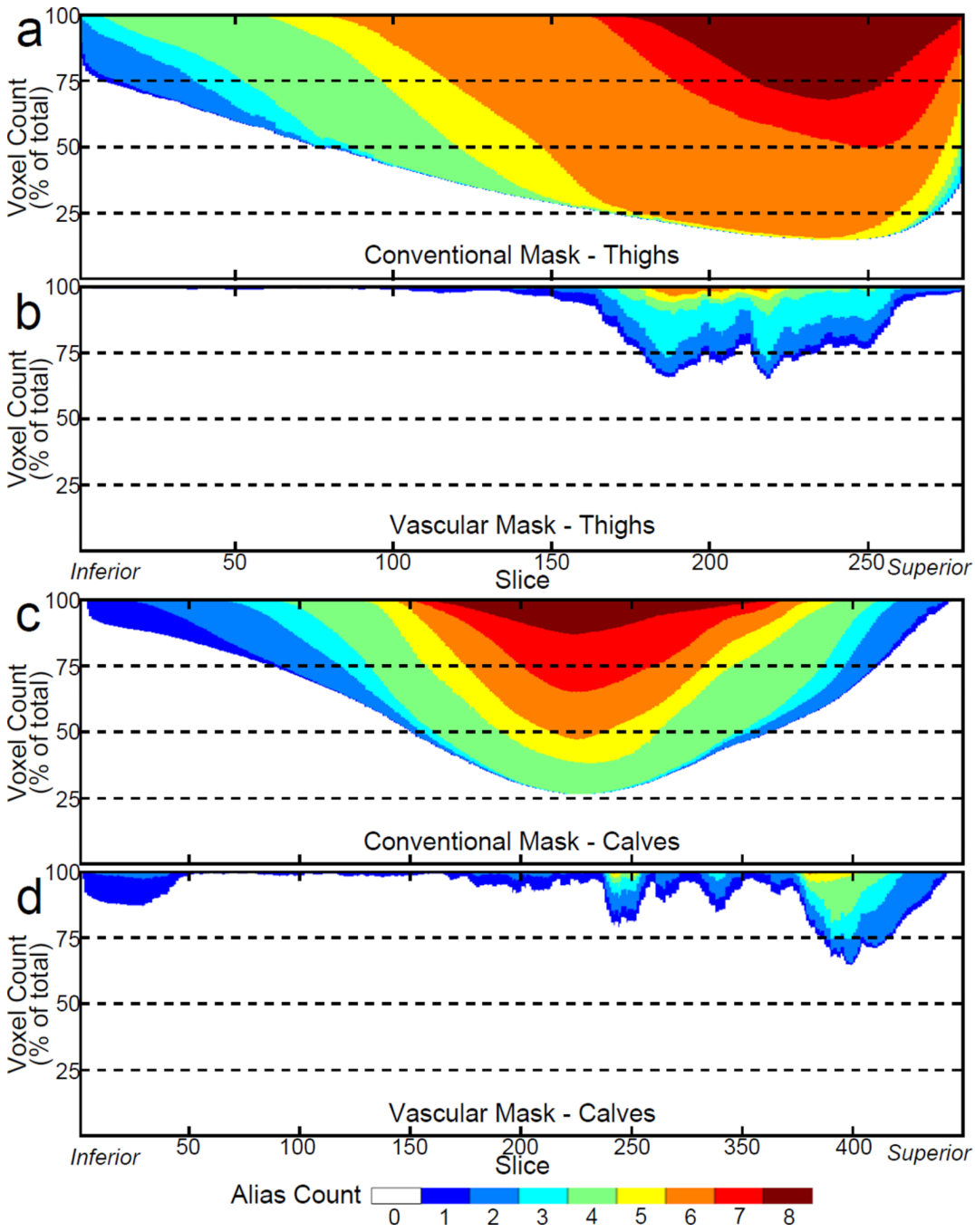

Figure 10.

Alias counts per axial slice for the thigh study shown in Figure 7 (a-b) and a calf study (c-d). Note that the vascular masking reduces the alias count per slice greatly and eliminates 7- and 8-fold aliasing.

Table 1

Typical CE-MRA Imaging Parameters

	Phantom	Thighs	Calves
Field of view (cm^3)	22.0 × 22.0 × 22.4	42.0 × 42.0 × 13.2	40.0 × 32.0 × 13.2
Sampling Matrix	224 × 224 × 224	280 × 280 × 88	400 × 320 × 132
Resolution (mm^3)	0.98 × 0.98 × 1.00	1.50 × 1.50 × 1.50	1.00 × 1.00 × 1.00
2D SENSE Acceleration ($R_Y \times R_Z$)	Varied	4 × 2	4 × 2
Homodyne Factor	1	1.9	1.8
Number and Arrangement of Receive Coil Elements	8 circumferential	12 circumferential	8 circumferential
TE (ms) / TR (ms) / FA (°)	2.1 / 6.5 / 30	2.0 / 4.7 / 30	2.7 / 5.7 / 30
Frame Time (s)	-	2.5	4.9
Temporal Footprint (s)	-	6.7	17.5
Subject Distribution (M/F)	-	4/17	6/7
Subject Age (years) (mean±s.d.)	-	47.0±18.0	53.6±11.2
Subject Weight (kg) (mean±s.d.)	-	77.5±16.4	84.4±17.8

Imaging parameters are included for phantom and in vivo studies. Field of view, sampling matrix, and resolution are reported as S/I × L/R × A/P.

Table 2

Review Criteria and Definition of Scores for Radiological Evaluation of in vivo Studies

Review Categories	
I.	**Depiction of Major Vessels**
	Compared to conventional masking, the depiction of major vessels in the composite image reconstructed with the vascular mask provides:
−2:	Reduced diagnostic confidence
−1:	Cosmetic/aesthetic degradation
0:	No improvement
1:	Cosmetic/aesthetic improvement
2:	Improved diagnostic confidence
II.	**Depiction of Small Vessels**
	Is there a loss of small vessels due to vascular masking in the composite image?
0:	No, no loss due to masking
1:	Yes, loss due to masking
III.	**Overall Assessment**
	Which image is preferred?
−1:	Prefer conventional image
0:	No preference
1:	Prefer composite image